Electronic Supplementary Material (ESI) for Materials Horizons.

Supplementary Information

Visualising compositional heterogeneity during the scale up of multicomponent zeolite bodies

A.J. Martin, S. Mitchell, K. Kunze, K.C. Weston and J. Pérez-Ramírez

Sorbent preparation. Li-X zeolite sorbents were prepared following the procedure described in US Patent 7300899. A low-silica zeolite X was first synthesised at industrial scale. Briefly, sodium silicate and sodium-potassium aluminate were added to a 1.5 m^3 autoclave water and mixed with a turbine to obtain a gel of composition $4.87Na_2O\cdot1.63K_2O\cdot2SiO_2\cdot Al_2O_3\cdot130H_2O$. The gel was allowed to ripen at 323 K for about 10 h and then crystallisation was carried out at 373 K for 4 h without agitation. The resulting solids were isolated by filtration, washed with water and dried at 333 K for 12 h in an air convection furnace. Chemical analysis of the solid evidenced a Si/Al ratio of 1.01. The zeolite powder was subsequently shaped with a highly dispersed attapulgite binder (10 wt.% dry weight) into milimetre-sized beads in a pan granulator (Eirich). The granules (coded K,Na-X) were subsequently hardened by calcination at 873 K for 2 h in a fluidised bed furnace. Lithium modification was achieved by ion exchange or the pre-formed zeolite granules in a single step with aqueous lithium chloride (1 M). After the ion exchange the resulting beads (coded Li-X) were washed, dried and calcined as described above.

Structural and textural characterisation. Inductively coupled plasma optical emission spectroscopy (ICP-OES) using a Horiba Ultima 2 instrument equipped with photomultiplier tube detection against a 5-point calibration curve. The granules were crushed and a small amount (0.1 g) was dissolved in mixtures of hydrofluoric acid (3 cm^3, 48 wt.% in H_2O, Sigma-Aldrich) and aqua regia (0.5 cm^3), followed by the addition of a saturated solution of boric acid (50 cm^3, Sigma-Aldrich, 99.5%) and water (45 cm^3). X-ray fluorescence (XRF) was conducted with an EDAX Orbis Micro-XRF analyser equipped with a Rh source and operated at a voltage of 20 kV and a current of 500 μA. X-ray diffraction was undertaken in a PANalytical X'Pert PRO-MPD diffractometer with Bragg-Brentano geometry using Ni-filtered CuKα radiation (λ = 0.1541 nm). The patterns were recorded in the 2θ range of 5-70° with an angular step size of 0.05° and a counting time of 8 s (standard) or 30 s (high resolution) per step. The granules were gently crushed prior to analysis. Ar isotherms at 77 K were measured in a Micromeritics TriStar II instrument. The whole granules were evacuated at 573 K for 3 h prior to measurement. The *t*-plot method was used to estimate the micropore volume and the mesopore (external) surface area. The mesopore volume was estimated by subtraction of the micropore volume from the total pore volume determined from the amount of Ar adsorbed at p/p_0 = 0.98. Pore size distributions were determined using nonlocal density functional theory models adjusted for Ar at 77 K in zeolites.

Mercury porosimetry was undertaken on whole granules with a Micromeritics Autopore IV 9510 following *in-situ* sample evacuation and using a contact angle of 140° and a pressure equilibration time of 10 s. The mesopore volume was determined from the amount of mercury intruded into pores of 3.8-50 nm, while the pore size distribution was derived by application of the Washburn equation.

Electron microscopy and energy-dispersive X-ray spectroscopy. Scanning electron (SEM) micrographs of the interior and external surface of the beads were aquired on a FEI Magellan 400 microscope working at 1 kV and 50 pA. The granules were studied whole or were first crushed and dispersed in dry form onto fresh carbon paint deposited on an aluminium holder. SEM and back-scattered electron (BSE) micrographs and energy-dispersive X-ray (EDX) spectroscopy maps of internal cross-sections were acquired on a Quanta 200F instrument. Sample preparation involved embedding granules in resin (LR white medium grade) and trimming and cutting the embedded granules with a high-precision rotating disk covered with diamond powder (Leika TXP), resulting in a surface roughness of <1 μm. Afterwards, the surfaces were polished by exposure to an argon ion beam (2 h, 4 kV, Hitachi IM4000). Finally, the samples were mounted on an aluminium holder and covered with a thin carbon film (*ca.* 5 nm) to prevent charging. Six granules per sample were initially studied by SEM to confirm the representativeness of the results. Subsequently, three cross-sections of each material were studied using a BSE detector to maximise the phase contrast, and finally, elemental maps were acquired by EDX from two representative samples. Scanning transmission electron (STEM) micrographs were acquired on a Talos F200X instrument operating at 200 kV and equipped with a high-angle annular dark-field (HAADF) detector as well as elemental an energy-dispersive X-ray spectrometer. Beam transparent sections (80 nm thick) were obtained from the resin-embedded granules ultramicrotomy, which were supported on copper grids coated with a continuous carbon film.

Nanoscale Secondary Ion Mass Spectrometry (NanoSIMS). The acquisition was carried out using a NanoSIMS 50L (Cameca) running at an operating pressure of $\sim 10^{-9}$ mbar. During NanoSIMS analysis a $^{133}Cs^{+}$ primary ion bean (16 keV) was rastered across the sample over a 30×30 μm area (256×256 pixels) with a 0.8 nA target current. Positive secondary ions generated by sputtering were extracted and analysed with high resolution according to their respective charge-to-mass ratios. Post-processing analyses were performed using the Open MIMS image plugin in the FiJi software with automatic drift correction. Sample preparation included the thermal pretreatment of the granules at 783 K for 4 h in static air, followed by immersing them in a resin with low degassing rate under ultra-high vacuum conditions (Epothin 2, Buehler), leaving them for 30 min to allow penetration of the resin into the granules and finally hardening the resin at room temperature. The resulting resin disks were consecutively polished with three different grades of silicon carbide (P400, P1200, P2000) until the interior of the granules was exposed.

The last step comprised finishing of the surface with alumina paste (0.05 μm) and cleaning in Millipore water for 2 h in an ultrasonic bath. A 50 nm thick gold coating was applied before measurement. For chemical mapping, secondary ions with nominal masses of 7 (Li), 23 (Na), 24 (Mg), 27 (Al) and 39 (K) a.u. are presented.

Table S1. Composition and porous properties of the samples.

Sample	Na/Al[a] (mol mol^{-1})	K/Al[a] (mol mol^{-1})	S_{ext}[b] (m^2 g^{-1})	V_{pore}[b] (cm^3 g^{-1})	V_{micro}[b] (cm^3 g^{-1})	V_{meso}[c] (cm^3 g^{-1})	V_{pore}[c] (cm^3 g^{-1})	d_{micro}[b] (nm)
Li-X	0.06	0.04	51	0.26	0.20	0.08	0.30	0.77
K,Na-X	0.73	0.27	27	0.20	0.17	0.04	0.29	0.75

[a] Determined by ICP-OES. [b] Determined by argon sorption. The *t*-plot method was used to estimate the micropore volume and the external surface area. [c] Determined by mercury porosimetry. The mesopore volume was determined from the amount of mercury intruded into pores of 3.8-50 nm.

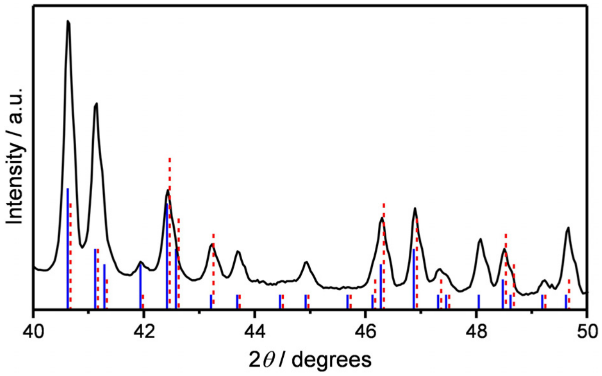

Figure S1. High-resolution XRD pattern (angular scan rate 0.1° 2θ min^{-1}) of the crushed K,Na-X granules. The vertical lines indicate reference peaks corresponding to zeolite X in potassium (red dashed line, $K_{66.56}Na_{21.66}(Al_{88}Si_{104}O_{384})\cdot(H_2O)_{7.137}$, JCPDS 01-070-4282) or sodium (solid blue line, $Na_{92}(Si_{100}Al_{92}O_{384})$, JCPDS 01-089-8235) forms.

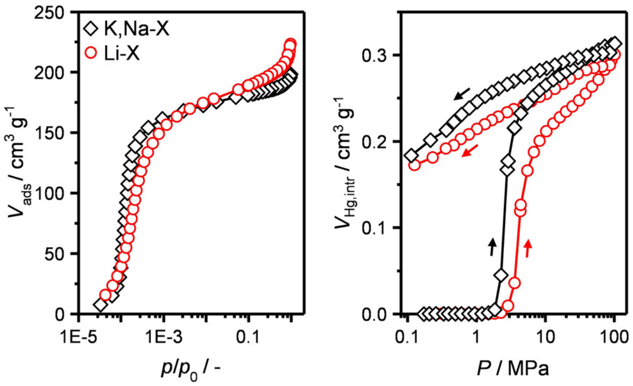

Figure S2. Argon isotherms at 77 K (left) and mercury intrusion/extrusion curves (right) of the K,Na-X and Li-X granules.

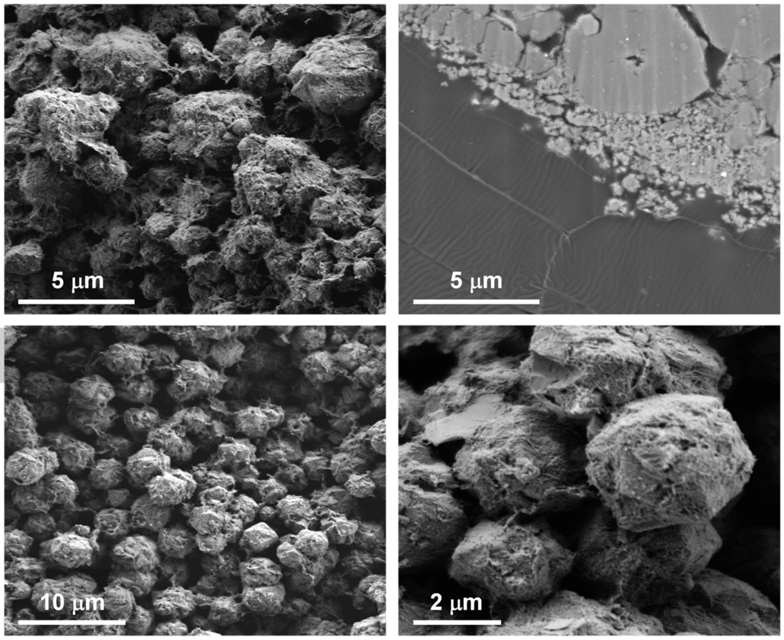

Figure S3. SEM micrographs of the surface (top left: top-down view of a whole granule, top right: cross-sectional view of an embedded granule) and interior (bottom row: images acquired from a crushed sample) of K,Na-X granules. The needle-like crystals of the attapulgite binder are seen to form a dense mat over the surface of the larger zeolite crystals which have a sphere-like morphology. No significant differences are noticeable between the external and internal particle organisation except that small particles (fines) are seen to coat the external surface in the cross-sectional image.

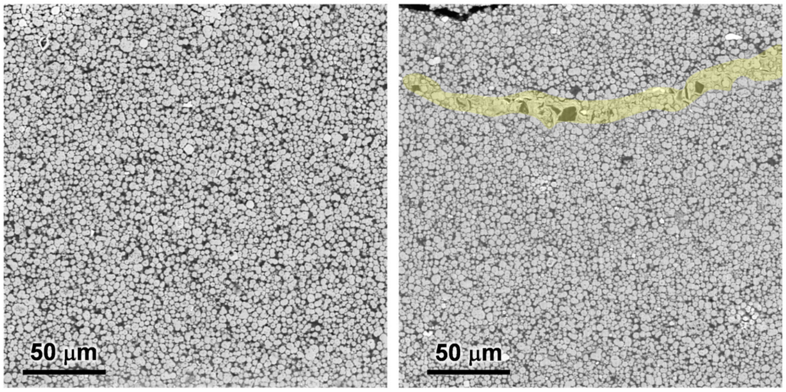

Figure S4. Low-magnification BSE micrographs of cross-sections through the center of K,Na-X and Li-X granules. Zeolite crystals of around 2-4 μm in diameter are seen to be closely packed and homogeneously distributed in both samples, the main distinction arising from the presence of a binder-rich zone (highlighted in yellow) in Li-X.

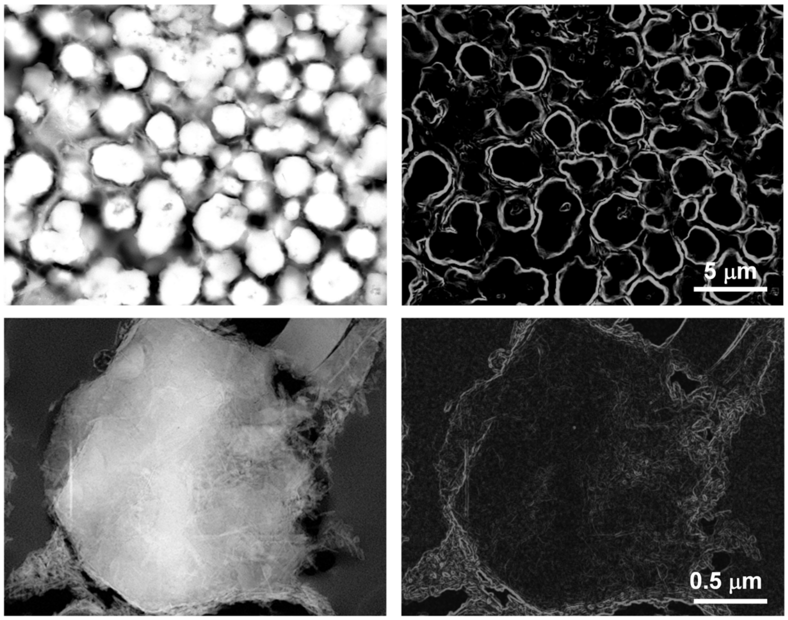

Figure S5. BSE (top left) and STEM (bottom left) micrographs of internal cross-sections of K,Na-X granules. The right column shows corresponding contour representations derived by image processing to identify particle locations in the elemental maps presented in **Figure 3** of the manuscript.

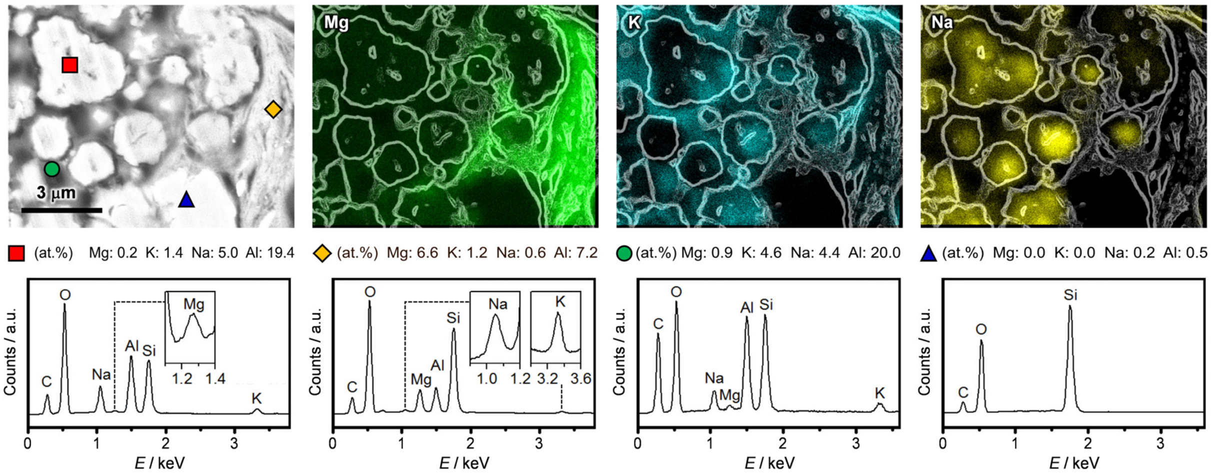

Figure S6. BSE micrograph of an internal cross-section of K,Na-X and corresponding elemental maps superimposed over a contour representation of the particle distribution (top row). EDX spectra at the positions indicated (bottom row). EDX data was acquired at 10 kV over 7 h resulting in *ca.* 1 μm penetration depth, attaining a higher spatial resolution than the data presented in **Figure 3** of the main manuscript (20 kV). Very similar distributions are confirmed for Mg and Na, but higher K signal is located within and around the periphery of zeolite particles. Note that an impurity silica particle (blue triangle) is also seen in the parent material.

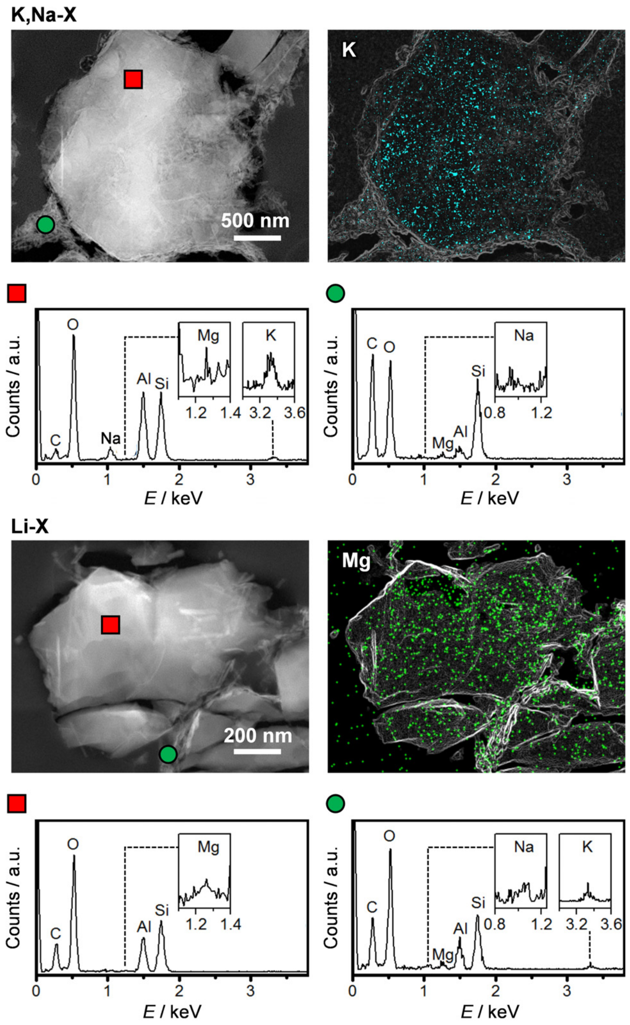

Figure S7. STEM images and corresponding elemental maps of K and Mg in thin cross-sections of the parent K,Na-X and Li-X granules. The EDX spectra obtained in zeolite-rich (red squares) and binder-rich (green circles) regions are also shown. Consistent with the respective compositions, a Si/Al ratio close to 1 is obseved over the zeolite, whereas the silicon content is higher over the binder. No Na or K remains in the zeolite after ion exchange, although trace amounts are evidenced in the binder. Mg is more noticeable in the binder, but is also detected in small amounts over the zeolite.

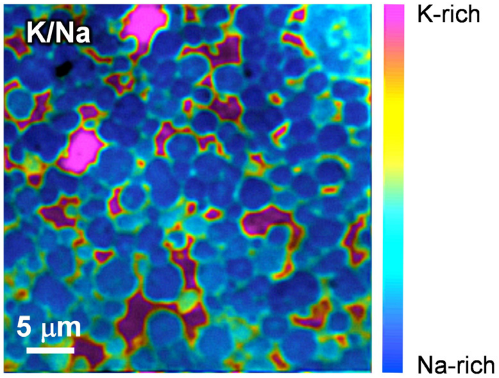

Figure S8. Relative distribution of K and Na over an internal cross-section of a K,Na-X granule. The map is calculated from NanoSIMS data based on the ratio of K^+/Na^+ ion signals per pixel after applying cut-off filters to avoid significant outliers.

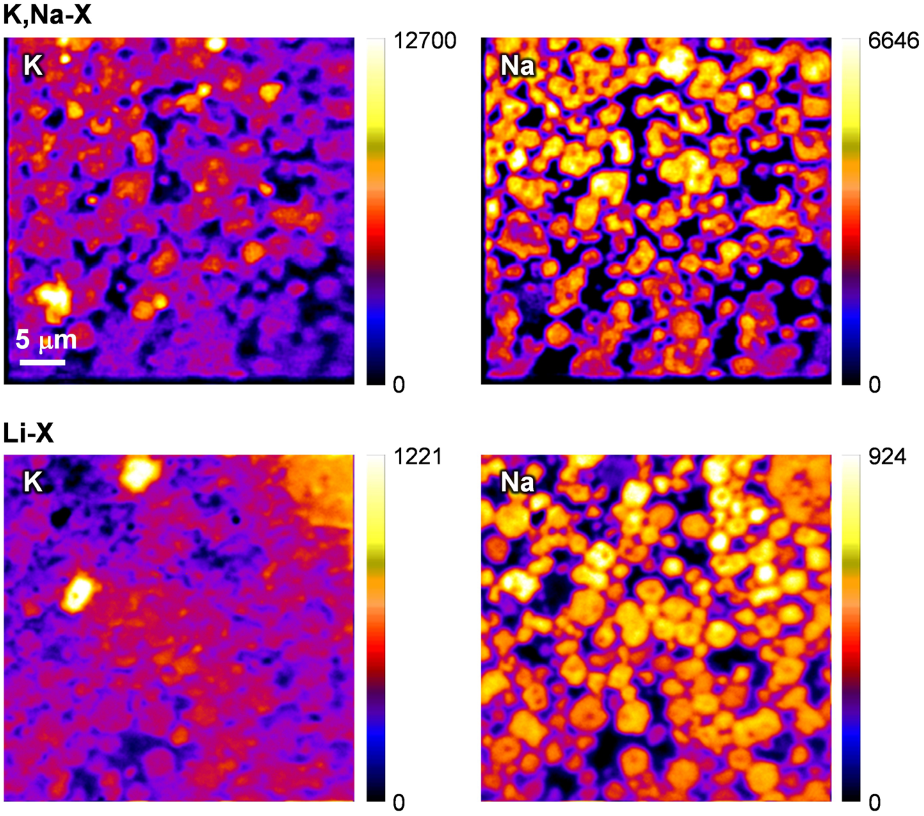

Figure S9. Chemical maps of K and Na acquired by NanoSIMS analysis of internal cross-sections of the K,Na-X (top row) and Li-X (bottom row) granules. Colour scales are normalised to the maximum number of counts (indicated in a.u.) per measurement. The comparative values clearly confirm the almost complete removal of Na and K upon exchange with Li.